



Impacts of two-dimensional and three-dimensional urban morphology on urban thermal environments in high-density cities: A case study of Hong Kong

Yong Xu^a, Jinxin Yang^a, Yingsheng Zheng^{b,*}, Wenjie Li^b

^a School of Geography and Remote Sensing, Guangzhou University, Guangzhou, China

^b College of Architecture and Urban Planning, Guangzhou University, Guangzhou, China



ARTICLE INFO

Keywords:

High-density cities
Urban morphology
Thermal environments
Two-dimensional
Three-dimensional

ABSTRACT

Urban morphology has a major effect on urban thermal environments, particularly in high-density cities, which are prone to urban environmental problems such as urban heat islands and air pollution. Thus, this effect must be understood to enable the formulation of effective climatic planning strategies to mitigate thermal threats in such cities. In this study, multi-sourced thermal data, namely remotely sensed land-surface temperature (LST) data and mobilely collected air-temperature (AT) data, are used to comprehensively analyze the contribution of urban morphology to urban thermal environments in neighborhoods in Hong Kong. The most widely used urban morphology parameters, such as floor area ratio, building coverage ratio, sky view factor, mean building height, road density, and vegetation coverage ratio, are assessed. Analyses of LST data and AT data indicated that the morphology parameters controlling urban thermal environments during the daytime differed from those controlling urban thermal environments during the nighttime. Specifically, at the neighborhood level during the daytime, the thermal environment is controlled by two-dimensional morphology parameters, such as impervious surface area, whereas in the nighttime, it is controlled by both two-dimensional and three-dimensional morphology parameters, such as sky view factor and road density. Moreover, an investigation of the performance and scaling effect of key morphology parameters indicated that such attributes have diversely sized influencing areas. The findings of this study will facilitate the formulation of urban design strategies for effectively reducing thermal threats in cities, thereby supporting the healthy and sustainable development of high-density cities.

1. Introduction

An urban heat island (UHI) is a well-known thermal phenomenon whereby an alteration of urban thermal properties and increased anthropogenic heat causes the air temperature (AT) or land-surface temperature (LST) in the central area of a city to be higher than the ATs or LSTs in its surrounding rural or suburban areas [1]. UHIs pose multiple threats to public health and well-being in cities, particularly in subtropical Asian cities, in which high temperatures on summer days are associated with an increased mortality rate [2]. In addition, an analysis of medical statistical data and meteorological observations from 2000 to 2015 in Hong Kong showed that reduced air ventilation and UHIs caused an excess mortality of almost 5.7% on summer days during this period [3]. Moreover, others have determined that an average increase of 1 K

above 29 °C was associated with a 4.5% increase in hospital admissions and that a daily mean temperature higher than 28.2 °C was associated with an approximately 1.8% increase in mortality in Hong Kong [4,5]. Thus, it is crucial to determine the urban morphology parameters controlling urban thermal environments, as this will allow effective climatic planning strategies to be devised and implemented to mitigate the adverse effects of UHIs and thus achieve sustainable development [6].

Initially, due to a limited number of weather stations, studies of urban thermal environments have mainly focused on temperature differences between urban and rural sites [7]. The key areas of investigation have included the causes and mechanism of UHIs, e.g., the contributions of climatic backgrounds and surface properties of specific locations to urban thermal environments [8,9]. Studies based on real-world observations have confirmed that land-surface attributes, such as the cooling effect of vegetation and the warming effect of

* Corresponding author.

E-mail addresses: xu1129@gzhu.edu.cn (Y. Xu), zhengyingsheng@gzhu.edu.cn (Y. Zheng).

Abbreviations

AT (T_a)	Air Temperature
BH (H)	Building Height
BCR (λ_b)	Building Coverage Ratio
FAR (λ_{floor})	Floor Area Ratio
FAD (λ_f)	Frontal Area Density
ISA (λ_i)	Impervious Surface Area
LCZ	Local Climate Zone
LST (T_s)	Land Surface Temperature
VCR (λ_v)	Vegetation Coverage Ratio
HW (λ_s)	Street-Width-to-Building-Height Ratio
MBH (z_H)	Mean Building Height
RD (λ_{road})	Road Density
RL (z_0)	Roughness Length
SVF (ψ_{svf})	Sky View Factor
2D	Two-dimensional
3D	Three-dimensional

impervious surfaces (quantified based on impervious surface area (ISA)), have substantial effects on urban thermal environments, although the spatial and temporal natures of these effects remain somewhat uncertain [10]. In addition, background climates and socio-economic activities have been found to have a profound influence on urban thermal environments [8,11]. Furthermore, well-developed microclimate simulation techniques and mobilely collected weather observations have been exploited to analyze the thermal performance of various urban areas, e.g., residential and commercial areas [12,13]. One of the most interesting findings was that land-cover configurations, in addition to land-cover compositions, play an important role in creating urban thermal environments, and this finding has important implications for district-based urban planning [14].

In current urban-climate research, there is a key knowledge gap between climatic knowledge (such as UHIs) obtained at the city level and the requirements of urban planning at the street level [6]. Strong evidence remains lacking regarding the associations between urban designs and climatic conditions, which restricts urban planners from developing effective planning strategies to facilitate sustainable development [6,15]. Take Hong Kong for example, its high-density and high-heterogeneity urban morphology at the neighborhood scale mainly comprises different built-up local climate zone types, from compact high-rise to open low-rise, which highlights the importance of a refined exploration of the influence of urban morphology on local climate conditions. According to a spatial sensitivity test of urban morphology in Hong Kong, the size of a neighborhood with a homogeneous urban form is about 200 m–300 m [16,17].

To formulate effective street- and community-level climatic planning strategies, an increasing number of studies have focused on examining urban climates at finer spatial scales (e.g., hundreds of meters) [6,15, 18]. For example, Stewart and Oke [19] conducted a pilot study in which they devised a novel local climate zone (LCZ) classification scheme that classifies urban structures into 17 standard classes, each of which has a unique thermal characteristic. The LCZ scheme is a fast and efficient way in which to understand urban thermal environments in urban neighborhoods and allows the translation of climatic knowledge into planning solutions at finer spatial scales than previous approaches. Thus far, the LCZ scheme has been applied successfully in various fields, including but not limited to urban planning, ecology, climatology, and geography [15,20]. Moreover, the LCZ scheme has been improved and further validated in recent years [21–24]. For example, Kotharkar et al. [21] found that the original LCZ scheme could be used only to examine thermal performance variations in LCZs with high heterogeneity and compact morphology, and thus devised a novel LCZ sub-classification

scheme to measure UHIs in some cities in India. Moreover, the use of AT measurement data to validate the thermal performance of standard LCZ classes has illustrated that some high-compact LCZ classes may exhibit large intra-class variations [22,23]. In contrast, other studies have used remote sensing-based LST data to evaluate and compare the thermal performance of various LCZs between cities ([25,26]; Jiang et al., 2021).

Furthermore, some scholars have examined the use of typical urban morphology parameters within LCZs to analyze urban thermal environments [27,28]. The most widely applied urban morphology parameters include three-dimensional (3D) morphology attributes, such as sky view factor (SVF), floor area ratio (FAR), and frontal area density (FAD), and two-dimensional (2D) morphology attributes, such as building coverage ratio (BCR) [18,29,30]. Reviews have determined that both 3D and 2D morphology parameters affect urban thermal environments, although there remain some uncertainties regarding the magnitude of their effects [31,32]. Moreover, a given urban morphology parameter may exhibit diverse performances in different districts within a city, and thus some studies have assessed the performance of key urban morphology parameters within different urban functional zones targeted for local solutions [13,29].

Key morphological parameters, such as SVF, can be used to measure UHI intensities [27,31,32]. However, existing knowledge about the performance and contribution of urban morphology to the thermal environment still has some uncertainties and limitations. First, studies have reported inconsistent or contradictory results on the performance of key morphology parameters and their contribution to urban thermal environments. For example, it was found that SVFs should be included when measuring thermal environments in high-density cities [33,34], whereas other studies have found that this is not the case in some other cities [27,35,36]. This inconsistency may be partly attributable to the use of different data, i.e., some studies have used LST data, whereas others have used AT data, as either type of data can well characterize urban thermal environments [31]. Second, most recent climatic studies have assumed that the magnitudes of the contributions of urban morphology parameters to urban thermal environments do not vary; however, the magnitudes of their contributions may vary from daytime to nighttime [32]. Moreover, it has not been determined which urban morphology parameters have the largest influence on urban thermal environments at the neighborhood level in high-density cities.

This study filled the above-mentioned knowledge gaps in urban climate research by employing multi-source thermal data to (1) identify urban morphology parameters that most affect urban thermal environments at the neighborhood level in high-rise and high-compact urban settings; (2) clarify the contribution of 2D and 3D urban morphology parameters to urban thermal environments based on both LST and AT data; and (3) evaluate the scaling effect and performance of key urban morphology parameters, and thereby determine their implications for urban planning. The contribution and performance of the most widely used urban morphology parameters, such as SVF, BCR, FAR, RD, and VCR, were examined. The findings should aid authorities in formulating effective climatic planning strategies for the sustainable development of high-density cities.

2. Study area and data sources

Hong Kong (22.4°N, 114.1°E) is located at the mouth of the Pearl River Delta in Southern China and has a humid subtropical climate, featuring a hot and humid summer and a relatively mild winter (see Fig. 1). Hong Kong consists of a group of islands and a peninsula that span an area of approximately 1000 km². Due to the hilly terrain and nature reservation policy of Hong Kong, its population of 7.5 million resides in only approximately 30% of its land area, which means that there is an extremely high population density in some areas. The average population density is approximately 6500 people/km², whereas that in the most densely populated places in some urban areas (e.g., Kwun

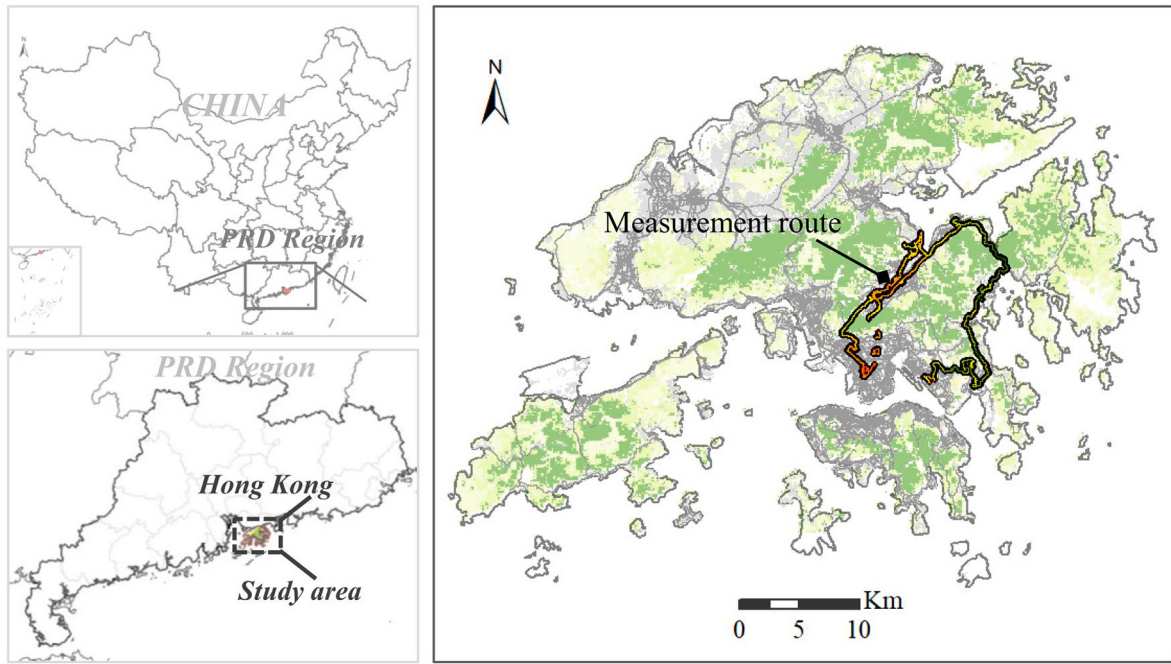


Fig. 1. Study area in Hong Kong (PRD = Pearl River Delta).

Tong) exceeds 50,000 people/km². In addition, the building density of Hong Kong is extremely high: the plot ratio is 5–6 on average and reaches a maximum of 12. Moreover, the average building height in Hong Kong is more than 50 m, according to 2010 building data [18]. The high population and building densities of Hong Kong mean that it suffers from environmental degradation associated with urban climate problems, such as UHIs and weak urban wind ventilation [2,6].

2.1. Datasets

The datasets used in this study contained built-environment data, satellite LST data, and mobilely collected AT data. The built-

environment data comprised precise urban geographic information system (GIS) data, such as 3D building and road network data, whereas the LST data were obtained from thermal satellite data, such as Landsat and Advanced Spaceborne Thermal Emission and Reflection Radiometer (ASTER) data. The AT data comprised temperature measurements made using a mobile data logger (testo-480) on typical summer days in various neighborhoods of Hong Kong. The quality of the satellite LST data and mobilely collected AT data have been validated in previous studies [26, 34]. Typical urban morphology parameters are included, namely SVF, FAD, FAR, BCR, street-width-to-building-height ratio (HW), mean building height (MBH), roughness length (RL), ISA, road density (RD), and vegetation coverage ratio (VCR).

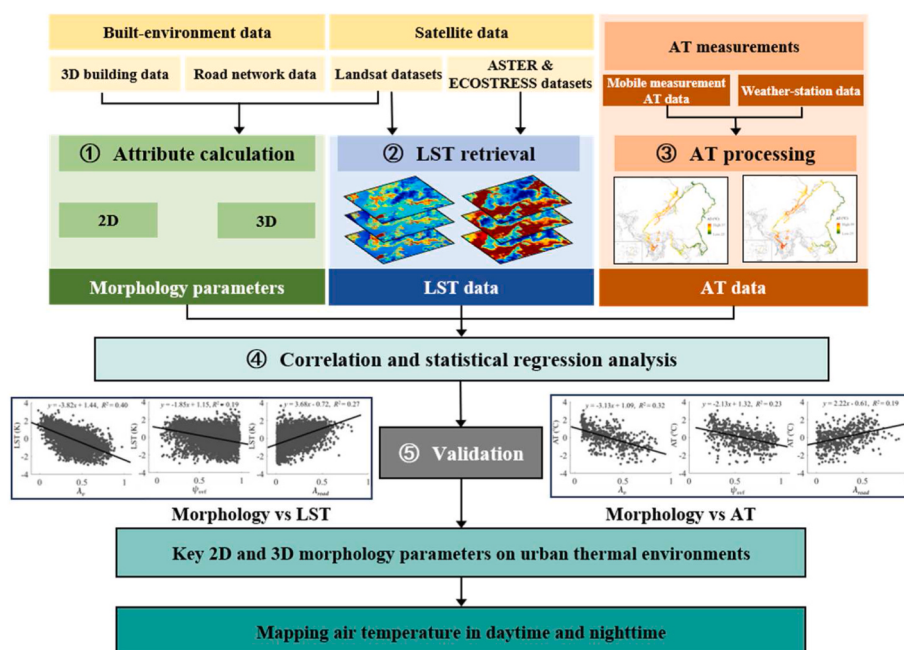


Fig. 2. The conceptual workflow of this study.

3. Methodology

The overall workflow of this study is displayed in Fig. 2. It mainly consists of five steps, including (1) calculation of urban morphology parameters, (2) LST retrieval, (3) AT processing, (4) correlation and regression analysis, and (5) validation. More details about each step are described in the following paragraphs.

3.1. Calculation of urban morphology parameters

The 10 typical urban morphology parameters that are calculated and used in this study are listed in Table 1. They comprised six 3D morphology parameters (i.e., SVF, FAR, FAD, MBH, HW and RL) and four 2D morphology parameters (i.e., ISA, BCR, RD and VCR) that have been confirmed to be associated with either LSTs or ATs [19,29,36–39]. Other than the 2D morphology parameters of ISA and VCR, which are calculated based on medium-resolution Landsat satellite data, all of the other 2D and 3D morphology parameters are calculated based on actual urban GIS data of Hong Kong.

All of the datasets are spatially aggregated into average values based on a defined grid at multiple-hundred-meter spatial resolutions (e.g., 200 m by 200 m), thereby ensuring that the morphology parameters are consistent and comparable. Fig. 3(a–f) depicts some sample SVF, BCR, RD, MBH, ISA, and VCR data, and reveals that their spatial distributions are consistent with actual situations; that is, the areas with the largest densities of buildings and roads are located in the most densely populated areas of Hong Kong, such as the Kowloon Peninsula region.

3.2. Satellite LST data

Hong Kong has a subtropical climate featuring long periods of cloudy or rainy days throughout the year, which meant that only a few clear-sky satellite datasets with thermal bands were available. Therefore, the overall thermal environment of Hong Kong was captured by using daytime satellite datasets, namely three Landsat datasets (for October 15, 2014, November 16, 2014, and February 7, 2016), and nighttime satellite datasets, namely two ASTER datasets (for December 16, 2015, and December 18, 2016) and one ECOSTRESS dataset (for November 15,

2019). The LST data were determined from the above-mentioned satellite data (see Fig. 4). For example, a single-channel algorithm was used to obtain actual LSTs from thermal band 10 of Landsat data, as band 11 was reported to have calibration problems [40]. In contrast, a temperature–emissivity separation algorithm was used to obtain actual LSTs from all five thermal bands in the 8–12-μm spectral range of the AST_08 LST product of ASTER datasets [41]. The retrieved LST datasets were recently verified [26,42].

3.3. AT measurements

A mobile measurement platform consisting of a light-colored multi-purpose vehicle equipped with microclimate sensors was utilized for mobile traverse measurements in this study. An air temperature/RH sensor probe was installed on the top of the van at approximately 2.5 m above the ground to monitor microclimate conditions at street level. The accuracy of the air temperature and RH sensor is ±0.3K and ±2%, respectively. The TESTO 480 data logger recorded data at 1-s intervals, while concurrently, the Garmin 62s GPS recorded both location and driving velocity at the same 1-s intervals. Two measurement routes were designed based on the LCZ classification map to cover the dominant LCZ types in Hong Kong. The total measurement time was limited to 2 h to control background weather condition changes.

The 6 days of measurements were performed on July 17, 2016, July 23, 2016, Aug 24, 2016, 25 Aug 2016, 27 Oct 2016, and 15 Aug 2017. According to the measured time, all the measurements are classified into two periods, namely a morning period (09:00–11:00) and an early-evening period (19:00–21:00), as shown in Fig. 5(a) and (b). In each period, the temporal adjustment was conducted based on the air temperature change rate recorded by nearby weather stations of the Hong Kong Observatory [22].

3.4. Statistical analysis

Both correlation and statistical regression methods are used to investigate the associations between urban morphology parameters and urban thermal environments. A correlation analysis is first performed using the nonparametric correlation method of Spearman, given that

Table 1
Definitions and calculations of urban morphology parameters.

Category	Attribute	Abbr.	Formula	Description
3D	Sky view factor (ψ_{svf})	SVF	$SVF = \frac{\sum_{i=1}^n SVF_i}{n}$ n: the number of SVF points in non-building areas;	Amount of sky that can be seen from the ground in an urban area (Chen, L. et al., 2010); median (IQR): 0.63 (0.46–0.78).
	Floor area ratio (λ_{floor})	FAR	$FAR = \frac{\sum_{i=1}^n S_{building}}{S_{site}}$ $\sum_{i=1}^n S_{building}$: the total floor area of the buildings;	Ratio of a building's floor area to the site area (in which the building is located); median (IQR): 6.29(2.34–13.01).
	Frontal area density (λ_f)	FAD	$FAD = \frac{\sum_{i=1}^n C_i}{S_{site}}$ C: the building frontal area.	Ratio of the building frontal area to the site area; median (IQR): 0.22 (0.09–0.43).
	Height-to-width ratio (λ_s)	HW	$HW = MBH/SW$ SW: the width of canyon street	Ratio of the mean building height to the width of the street abutting the building; median (IQR): 3.04 (1.68–5.65).
	Mean building height (z_H)	MBH	$MBH = \frac{\sum_{i=1}^n BS_i * H_i}{\sum_{i=1}^n BS_i}$ BS _i : the ground area of a building;	Average building height in a site area; median (IQR): 41.99 (22.11–74.14).
	Roughness length (z_0)	RL	$RL = MBH * \frac{C_d}{0.74} * \left(1 - \frac{Z_d}{H}\right)^2 * \frac{FAD}{BCR}$ C_d : the drag coefficient; Z_d : zero displacement height.	A measure of the roughness of a surface over which a fluid is flowing (Xu. et al., 2017); median (IQR): 3.29 (0.75–9.15).
2D	Impervious surface area (λ_i)	ISA	$ISA = \frac{\sum S_{per}}{S_{site}}$	Ratio of the impervious surface area to the site area; median (IQR): 0.44 (0.40–0.47).
	Building coverage ratio (λ_b)	BCR	$BCR = \frac{\sum_{i=1}^n BS_i}{S_{site}}$	Ratio of the building coverage area to the site area; median (IQR): 0.14 (0.07–0.23).
	Road density (λ_{road})	RD	$RD = \frac{S_{road}}{S_{site}}$	Ratio of the road area to the site area; median (IQR): 0.17 (0.07–0.29).
	Vegetation coverage ratio (λ_v)	VCR	$VCR = \frac{S_{vegetation}}{S_{site}}$	Ratio of the vegetation area to the site area; median (IQR): 0.36 (0.23–0.49).

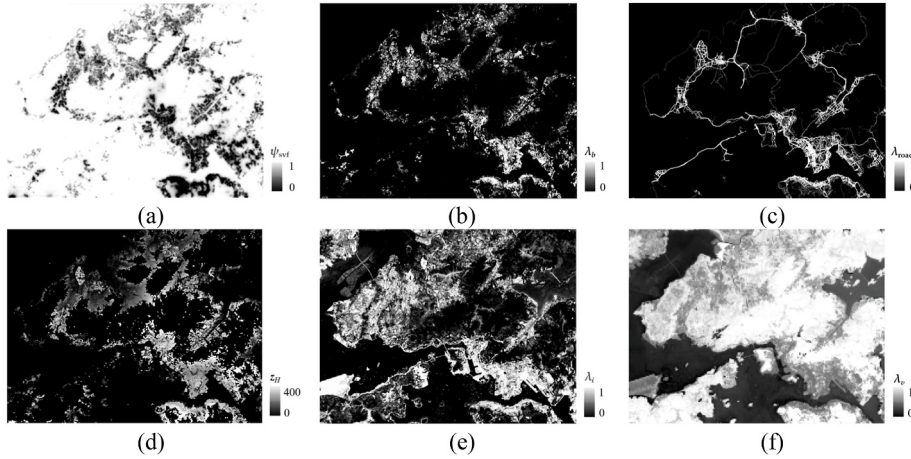


Fig. 3. Sample urban morphology data for Hong Kong. (a)SVF (ψ_{svf}); (b) BCR (λ_b); (c) RD (λ_{road}); (d) MBH (z_H); (e) ISA (λ_i); and (f) VCR (λ_v).

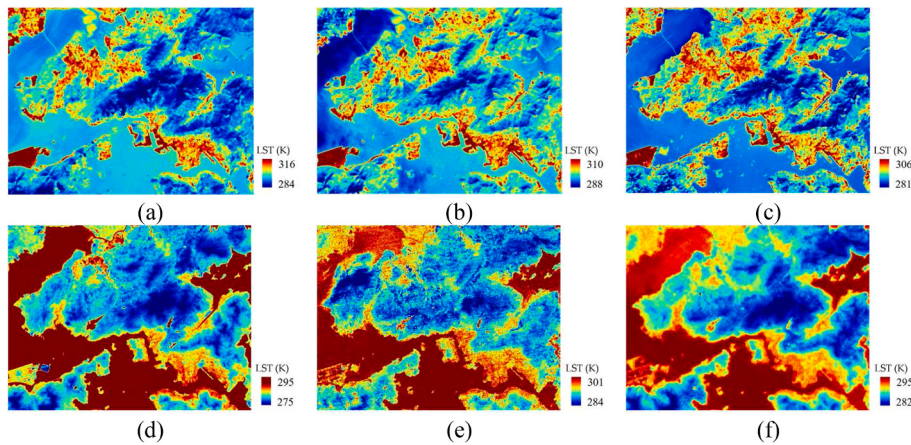


Fig. 4. LST data for Hong Kong determined from (a) daytime Landsat data on October 15, 2014; (b) daytime Landsat data on November 16, 2014; (c) daytime Landsat data on February 7, 2016; (e) nighttime ASTER data on December 16, 2015; (e) nighttime ASTER data on December 18, 2016; and (f) nighttime ECOSTRESS data on November 15, 2019.

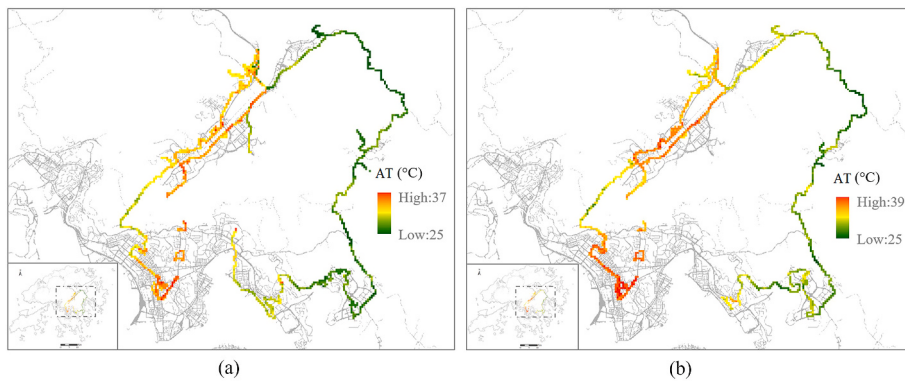


Fig. 5. Mobile air temperature measurements made during a typical summer's day in Hong Kong in (a) the morning (9:00–11:00); and (b) the early evening (19:00–21:00).

some of the morphology parameters may not be linearly correlated. As recommended by previous studies [17,19], hundreds of meters resolution is an optimized scale to effectively capture the spatial heterogeneity and thermal characteristics of built environments in Hong Kong. Thus, the whole study area is divided into a grid comprising 200 m × 200 m cells, and thousands of valid values are obtained for each variable (i.e., the urban morphology parameters and temperatures).

Subsequently, multiple linear regression and stepwise linear regression methods are used to analyze the contribution of the morphology parameters to urban thermal environments at the neighborhood level. The conventional linear regression model can be expressed as follows:

$$y = \beta_0 + \beta_1 \times x_1 + \beta_2 \times x_2 + \dots + \beta_i \times x_i + \varepsilon$$

where β_i is the regression coefficient of the i th urban morphology

parameter, x_i is the i th urban morphology parameter, and y is the LST or AT in a given area.

The above-mentioned linear regression model is used as the basis for the step-by-step construction of a linear regression model. In each step, the statistical significance of each independent variable is tested, such that potential explanatory variables could be added or removed in each iteration. After several rounds of iterations, the most appropriate combination of variables is selected for use in the final model.

3.5. Model validation

By comparing with actual observations, both the root-mean-square error (RMSE) and adjusted R^2 are calculated to assess the modeling capability as well as the cross-validation of the resultant models. Both indices could be calculated as below:

$$\text{Adj } R^2 = 1 - (1 - R^2) \left(\frac{n - 1}{n - p - 1} \right)$$

$$\text{RMSE} = \sqrt{\frac{1}{n} \sum_{i=1}^n (\tilde{T} - T)^2}$$

Where R^2 is the coefficient of determination of regression models. n is the number of statistical points, and p is the total number of used morphology variables. T is the measured surface or air temperature, while \tilde{T} is the estimated temperature from the proposed models.

Given the limited mobile-based measurements, leave-one-out cross-validation (LOOCV) is used to evaluate all the modeling results. Particularly, a 5-fold cross-validation is used, in which all dataset is split into five parts, one part is used as a validation set and the other four parts are used as training data. The validation process is repeated five times, and at each time one part is in turn used as validation data and the remaining parts as training data. The final adjusted R^2 and RMSE could be calculated based on the results at each time.

4. Results

4.1. Correlation analysis for variable selection

A Spearman correlation analysis is performed using all of the values

for each variable to investigate the associations between urban morphology parameters and LSTs and ATs. Fig. 6 shows the Spearman correlation coefficients of the associations between the 10 urban morphology parameters and the temperatures during both the daytime (the upper four rows) and the nighttime (the lower four rows).

As expected, most of the urban morphology parameters are significantly correlated with both LSTs and ATs, except for a few 3D morphology parameters (i.e., SVF) during the daytime. In addition, VCR is negatively correlated with both LSTs and ATs, which is consistent with the results of some other studies [43,44]. Moreover, the results indicated that both 2D and 3D urban morphology had significant warming effects on urban environments during the nighttime, as a 2D morphology parameter (RD) and a 3D morphology parameter (FAR) are strongly correlated with nighttime LSTs and ATs. In contrast, 3D urban morphologies tend to have a cooling effect on urban environments during the daytime, as a 3D morphology parameter (MBH) is negatively correlated with both LSTs and ATs. Moreover, the results reveal that RD is strongly correlated with urban thermal environments during both the daytime and nighttime, indicating that the contribution of road networks to urban thermal environments could not be ignored in this study.

4.2. Regression for model construction

Next, a stepwise regression model is employed to identify the morphology parameters that are most important for modeling urban thermal environments during the daytime and nighttime. Various selection strategies, e.g., backward, forward, and bidirectional strategies, are used, and the essential morphology parameters are those that are selected by all of the strategies.

Table 2 shows the stepwise regression results for the morphology parameters during the daytime and nighttime in Hong Kong. LSTs and ATs are taken as independent variables to reflect urban thermal environments, and multiple morphology parameters are taken as predicted variables. The results reveal that the most important urban morphology parameters are SVF, RL, RD and VCR, as they are consistently selected for modeling either LSTs or ATs. Other morphology parameters, such as HW, MBH, ISA, and BCR, are required for modeling LSTs but not for modeling ATs. Thus, distinct morphology parameters primarily affect ATs and LSTs, respectively. LST data are well explained by morphology parameters, as the coefficients of determination (R^2) of LST data with

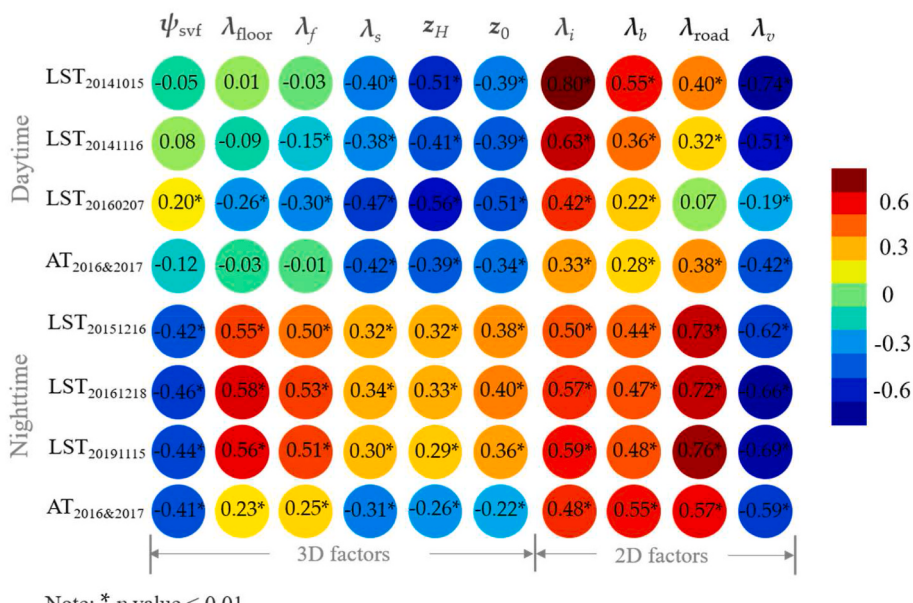


Fig. 6. Spearman correlation coefficients between the selected urban morphology parameters and land surface temperature (LSTs) and air temperature (ATs) during daytime and nighttime.

Table 2

Stepwise regression results (e.g., standardized regression coefficients and coefficients of determination (R^2) for multiple satellite land-surface temperatures (LSTs) and mobilely collected air temperatures (ATs) and morphology parameters in Hong Kong.

Parameters	Standardized regression coefficients							
	Daytime				Nighttime			
	LST ₂₀₁₄₁₀₁₅	LST ₂₀₁₄₁₁₁₆	LST ₂₀₁₆₀₂₀₇	AT _{2016&2017}	LST ₂₀₁₅₁₂₁₆	LST ₂₀₁₆₁₂₁₈	LST ₂₀₁₉₁₁₁₅	AT _{2016&2017}
3D	SVF (ψ_{svf})	0.20**	0.26**	0.46**			-0.11*	-0.11*
	FAD (λ_f)	-0.35**	-0.23**		0.62**	0.34**	0.39**	-0.36**
	FAR (λ_{floor})			-0.25**		0.37**	0.23**	-0.28**
	MBH (z_H)	-0.27**			-0.38**	-0.37**	-0.55**	-0.49**
	RL (z_0)	0.34**				-0.43**	-0.19**	-0.27**
2D	ISA (λ_i)	0.78**	1.03**	0.96**		0.43**	0.38**	0.43**
	BCR (λ_b)	0.26**	0.25**	0.23**		-0.37**	-0.30**	-0.34**
	RD (λ_{road})				0.17**			0.23**
	VCR (λ_v)		0.46**	0.66**	-0.21*	-0.71**	-0.62**	-0.69**
No.		752	752	752	172	752	752	150
R^2		0.83	0.61	0.62	0.36	0.65	0.64	0.47

Notes. 3D = three-dimensional; 2D = two-dimensional.

morphology parameters are all greater than 60% during the daytime and the nighttime. In contrast, AT data are less well explained by urban morphology, as the R^2 of AT data with urban morphology is only 50%, which indicates that the modeling of AT is more uncertain than the modeling of LST at the neighborhood level.

4.3. Accuracy assessment

Based on 5-fold cross-validation, the overall accuracies of the predicted temperatures can be obtained by comparing them with the actual observations from either satellite-based LSTs or mobile-based ATs. Fig. 7 shows the accuracy statistics of adjusted R^2 and RMSE for all the regression models listed in Table 2, in which a higher adjusted R^2 and a lower RMSE value indicate that the temperatures are modeled with higher quality. When compared with street-level air temperature, the

surface temperature is predicted much better, as the RMSEs are lower than these figures for air temperature simulations. Moreover, the results reveal that urban morphology performs better in modeling the nighttime thermal environment than the daytime environment, as all the obtained RMSEs during the nighttime are relatively smaller than these figures in the daytime, reflecting that nighttime urban thermal environments might be better explained by the local urban morphology.

4.4. Air temperature mapping in daytime and nighttime

The regression models between the important urban morphology parameters (e.g., RD and ISA) and temperature observations are used to simulate the temperature distributions over the entire study area. Fig. 8 (a) and (b) show the simulated daytime and nighttime ATs, respectively, of Hong Kong. These ATs are simulated based on the AT models

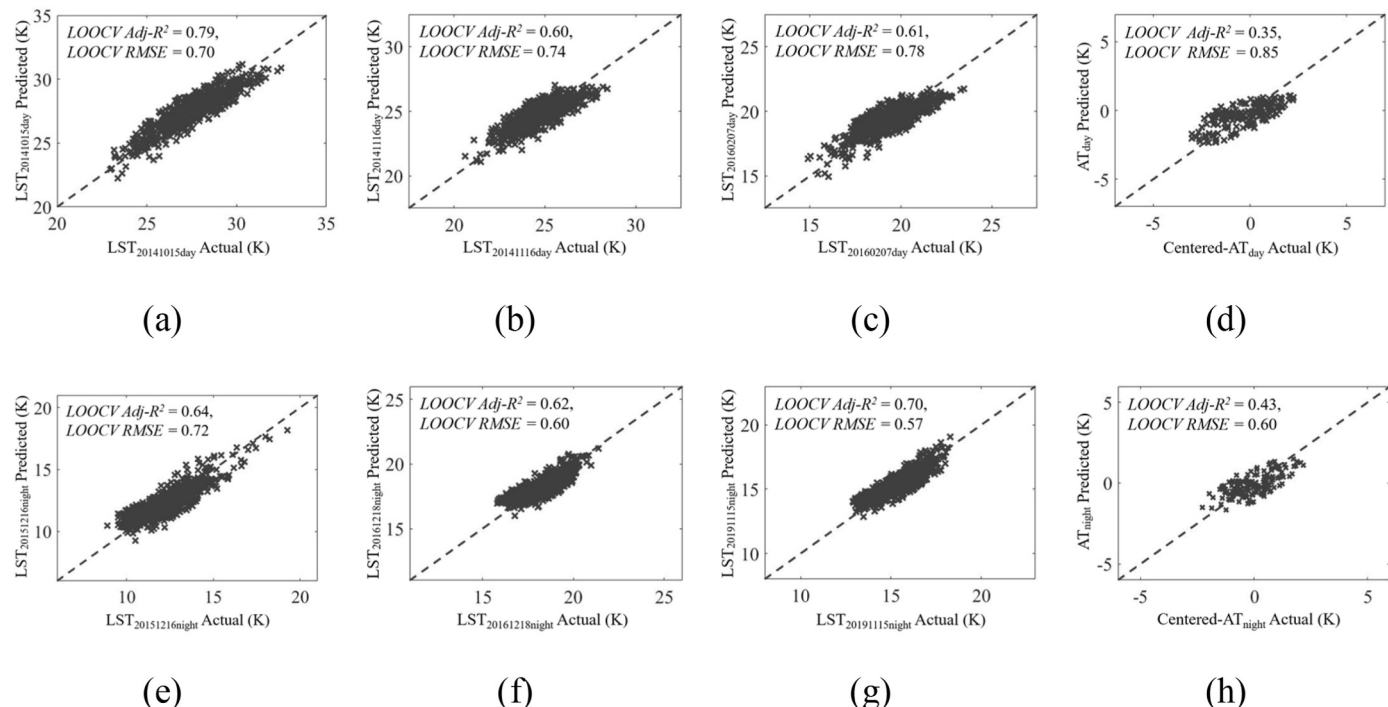


Fig. 7. Validation of different regression models by comparing the predicted temperatures with the actual observations from either satellite-based LSTs or mobile-based ATs based on 5-fold LOOCV validation method. (a) daytime LST on Oct 15, 2014; (b) daytime LST on November 16, 2014; (c) daytime LST on February 7, 2016; (d) daytime AT (9:00–11:00); (e) nighttime LST on December 16, 2015; (f) nighttime LST on December 18, 2016; and (g) nighttime LST on November 15, 2019; and (h) nighttime AT (17:00–19:00).

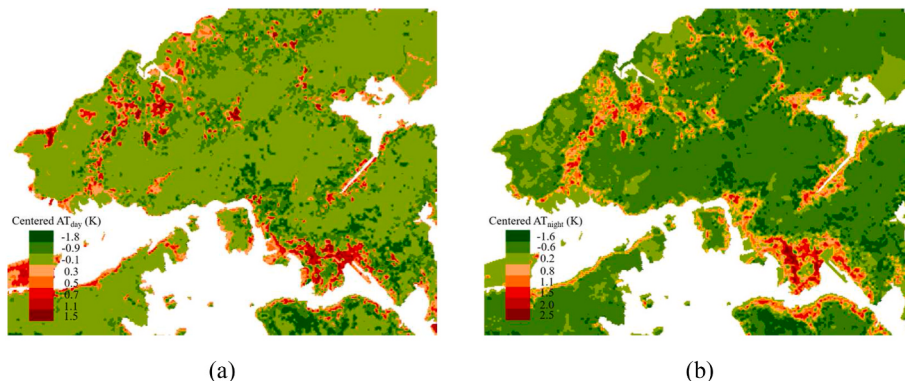


Fig. 8. Simulated zero-centered air temperatures (ATs) at Hong Kong in both daytime and nighttime using the devised models. (a) Simulated daytime AT; (b) Simulated nighttime AT.

provided in columns 5 and 9 of **Table 2**: daytime AT is simulated using RL, VCR, and RD, whereas nighttime AT is simulated using SVF, MBH, VCR, and RD.

The simulated results in Fig. 8 clearly show that the ATs in urban areas are higher than those in rural areas and that the distribution of ATs is highly consistent with the distribution of human settlements in Hong Kong. For example, Kowloon Peninsula, a high-density urban area, has a much higher AT than the other areas. Thus, these results reveal the pattern of UHIs and that their extent expanded significantly from daytime to nighttime, i.e., the areas of overheated regions increased greatly from daytime to nighttime, particularly in some built-up regions near to water and greenery.

5. Discussion

This study identified some key urban morphology parameters and developed empirical models that can be used to simulate urban thermal environments in Hong Kong. The results of regressions based on both satellite LSTs and mobilely collected ATs highlight that several urban morphology parameters, such as SVF, MBH, RD and VCR, are essential for modeling urban thermal environments in Hong Kong. These essential morphology parameters could be classified into two categories: 3D morphology parameters (e.g., SVF and MBH), and 2D morphology parameters (e.g., BCR and RD). The results enhance our understanding of how 3D and 2D morphologies affect urban thermal environments, and provide insights for the development of planning recommendations for heat mitigation in cities. The performance and uncertainties of the urban morphology parameters and their implications for urban climate studies are discussed below.

5.1. Contribution of 2D and 3D urban morphology to urban thermal environments

The correlation and regression analysis results mentioned in the

above sections 4.1 and 4.2 confirmed that some 2D and 3D urban morphology parameters make a substantial contribution to urban thermal environments. Specifically, SVF, RD, MBH and VCR are strongly correlated with both LSTs and ATs. Scatterplots with fitted lines are constructed to investigate these building attributes' effects on urban thermal environments, as reflected by satellite LSTs and mobilely collected ATs. These scatterplots are depicted in Figs. 9 and 10, respectively, and their x - and y -coordinates represent the morphology parameters and zero-centered temperature, respectively. The R^2 is also provided for each attribute to reveal how closely the points fit the trendline.

The results show that the effects of morphology parameters on urban thermal environments, in terms of both satellite LSTs and mobilely collected ATs, are consistent. For example, the SVF and RD results reveal that the temperatures of urban environments increased as the density of urban morphology increased. In addition, an increase in the VCR has a well-defined cooling effect, as both LST and AT could decrease by about 0.3 K when the vegetated coverage ratio increases by 10%. Similar findings have been recorded in previous studies [43,44]. Moreover, MBH is found to have a complex effect on urban thermal environments: an increase in MBH first caused an increase in LST and AT, but further increases in MBH (to ~40 m) caused a decrease in LST and AT.

The above-described nonlinear relationship between MBH and LST and AT suggested that the relative contribution of MBH and other morphology parameters to urban thermal environments may be better quantified by a nonlinear regression method than by a linear regression model. The random forest method is effective for determining the contributions of various features based on their Gini importance [18]. Thus, the Gini importance of each morphology parameter is used to determine the normalized contribution of the attributes to urban thermal environments during the daytime and nighttime, respectively, as shown in Fig. 11 (a) and (b).

An analysis of the above-mentioned results indicates that the morphology parameters most affecting urban thermal environments

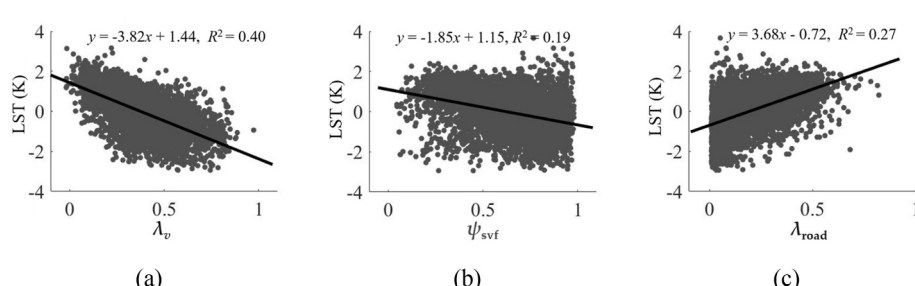


Fig. 9. Effect of morphology parameters on land-surface temperature (LST) with respect to (a) VCR (λ_v); (b) SVF (ψ_{svf}); and (c) RD (λ_{road}) (R^2 = coefficient of determination).

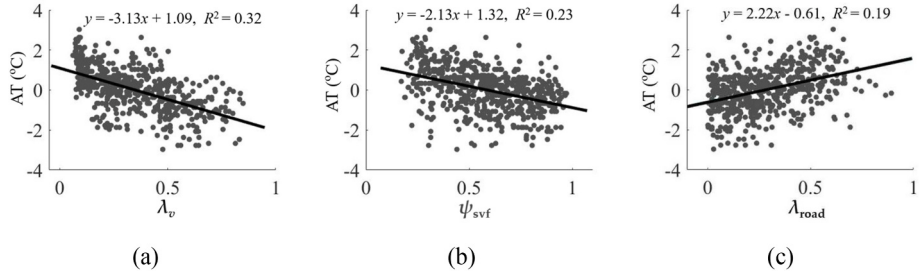


Fig. 10. Effect of morphology parameters on air temperature (AT) with respect to (a) VCR (λ_v); (b) SVF (ψ_{svf}); and (c) RD (λ_{road}) (R^2 = coefficient of determination).

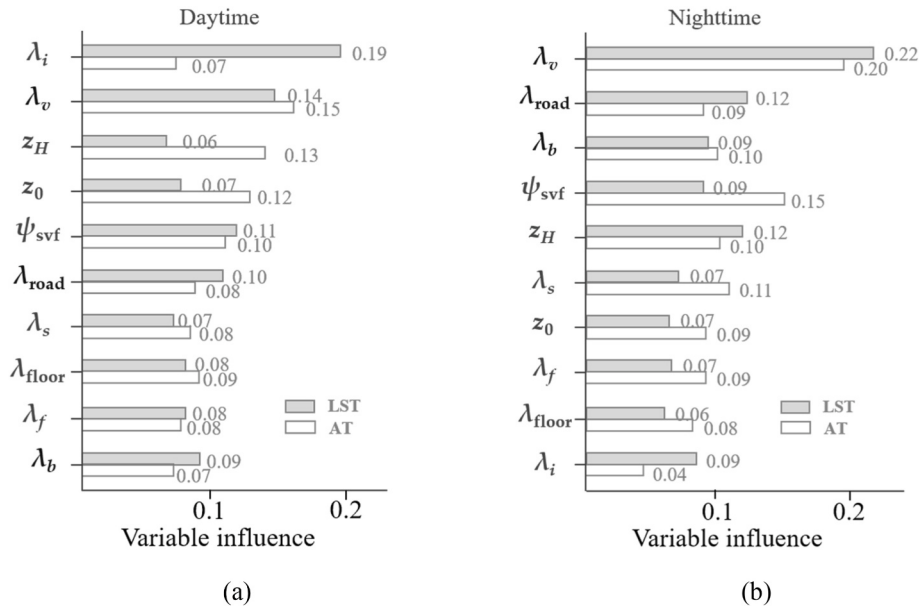


Fig. 11. Relative importance of the effect of various morphology parameters on urban LSTs and ATs during the (a) daytime and (b) nighttime.

differ from daytime to nighttime. Specifically, 2D morphology parameters contribute most to urban thermal environments during the daytime, whereas both 2D and 3D morphology parameters contribute to urban thermal environments during the nighttime. Moreover, during the daytime, the morphology parameters that most affected AT differ from those that most affected LST, whereas during the nighttime, almost the same attributes most affected AT and LST. Furthermore, ISA contributes the most to daytime LST but makes a near-negligible contribution to nighttime LST. The results also reveal that the distributions of LST and AT at nighttime are highly consistent, indicating that nighttime satellite LST data could be used for quantifying UHIs.

5.2. Scale effect

The scale effect of the influence of various morphology parameters on urban thermal environments is determined by examining the correlation between key attributes and LSTs and ATs over various scales. Sufficient samples are obtained for a valid statistical analysis by using 10 different scales (from 100 m to 1000 m) for LSTs, and four different scales from 100 m to 400 m for ATs. The tested attributes comprise all of the important 2D and 3D morphology parameters, such as SVF and RD, which are proven to make a large contribution to urban thermal environments.

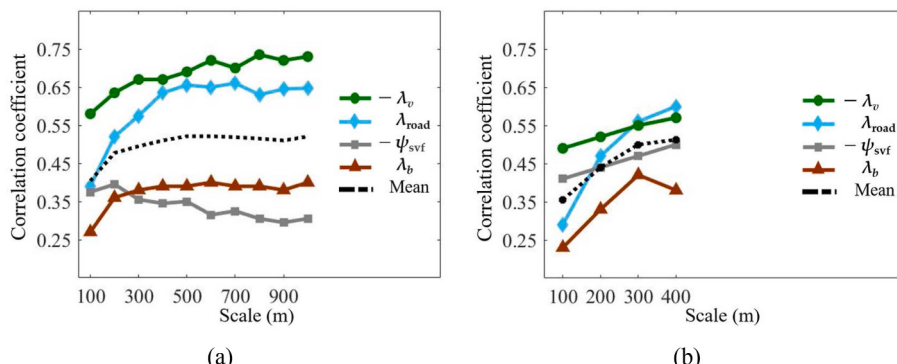


Fig. 12. Plots of Spearman correlation coefficients between important morphology parameters (VCR (λ_v), RD (λ_{road}), SVF (ψ_{svf}), BCR (λ_b) and their mean) and the thermal environment expressed as (a) LST; and (b) AT.

Fig. 12(a) and **(b)** show the Spearman correlation coefficients between urban thermal environments and the important morphology parameters at various scales, and reveal two major relationships. First, different morphology parameters have different influencing areas. In particular, the 2D attributes (e.g., RD and VCR) have a larger influencing area than the 3D attributes (e.g., SVF). These relationships exist between morphology parameters and both LST data and AT data, although the latter might have contained some uncertainties, due to the limited sample size of AT data at large scales. Second, the optimal scale is found to be approximately 200–300 m; at this scale, both 2D and 3D morphology parameters have effects, and the spatial details of thermal characteristics are well preserved.

5.3. Implications for urban climate studies

The LCZ classification scheme serves as a standard and efficient way to understand urban thermal environments at the neighborhood scale in some low-rise cities. However, the thermal performance of various LCZs in high-density urban settings needs further investigation [21]. In the current study, we collected and analyzed multiple field-measurement AT data and found that the standard LCZs effectively differentiated between urban thermal environments in high-rise and highly compact urban settings. As indicated in **Fig. 13**, urban LCZs have contrasting thermal performance; in particular, the average AT of highly compact urban LCZ classes (e.g., LCZs 1–3) is significantly higher than that of the open LCZ classes (e.g., LCZs 4–6). This confirms that compared with dense LCZ classes, open LCZ classes with more vegetation have a lower AT. These results are highly consistent with the findings of some other studies [22,26].

We also assessed the contributions of various morphology parameters to urban thermal environments to identify the morphology design factors that are most important for urban planning. Some of our findings are novel and thus contribute to LCZ knowledge. First, we found that the effect of urban morphology on urban thermal environments can be dynamic and nonlinear. For example, the overall contribution of MBH, a 3D morphology factor, to urban thermal environments varied over time; a high MBH had a cooling effect in the daytime but a warming effect in the nighttime. Moreover, ATs increased as the MBH increased in the nighttime, but ATs decreased after the MBH reached a certain threshold. This may explain why some compact LCZs with different MBHs can exhibit similar ATs, such as LCZs 1 and 2 in this study. Second, we found that a high RD caused substantial warming at the neighborhood level, both during the daytime and the nighttime. This warming effect of high RDs has rarely been mentioned in standard LCZ studies of some other cities [34,45]. Given the above-mentioned findings, MBH and RD were adjusted and used to simulate a set of predicted ATs for standard LCZs, as depicted in **Fig. 13**. It can be seen that the simulated ATs more effectively differentiated LCZs than did the observed ATs. These findings indicate that spatial planning strategies for high-density cities, such as

Hong Kong, must consider adjusting some morphology parameters, such as RD and MBH, when applying the original LCZ scheme.

6. Conclusion

This study employed multiple remote-sensing-based LST data and mobilely collected AT data to assess the effect of various urban morphology parameters on urban thermal environments and the attributes' performance over space and time. The results clarify how urban morphology affects urban thermal environments and identify the most important urban morphology parameters for consideration in urban design, particularly for some high-density cities.

The statistical analysis results confirmed that certain morphology parameters have major effects on urban thermal environments at the neighborhood level, although the dominant attributes can change over time. In addition, a novel finding was that the dominant attributes that affected urban thermal environments during the daytime differed from those that did so during the nighttime. Analogously, the dominant attributes that affected LSTs differed from those that affected ATs. Specifically, urban thermal environments during the daytime were mainly affected by 2D morphology parameters (e.g., ISA) during the daytime but by both 2D and 3D morphology parameters (e.g., FAR and RD) during the nighttime. Moreover, during the nighttime, the LST was mainly affected by FAR and RD, but the AT was mainly affected by SVF and RD.

This study also clarified the performance of key morphology parameters and their scale effects, which have implications for urban planning. First, the application and utility of standard LCZs for describing high-density urban settings were reassessed. The performance analysis results showed that the warming effect of high RDs has been severely underestimated in previous studies, which implies that the effect of high RDs should be considered in high-density urban designs for UHI mitigation. Second, the scale analysis results indicate that morphology parameters have a diverse influencing range; for example, 3D morphology parameters (e.g. SVF and MBH) tended to have much smaller influencing ranges (<200 m) than 2D morphology parameters (>500 m). This result implies that urban designs should consider the cooling or warming effect of various morphology parameters over a range of scales.

In summary, this study revealed the different impacts of two-dimensional and three-dimensional urban morphology on daytime and nighttime urban heat conditions in the high-density urban environment of Hong Kong. The quantitative understanding of the connections between urban morphology parameters and urban heat conditions could provide a reference to formulate reasonable spatial planning and morphology design solutions for sustainable urban development in high-density cities.

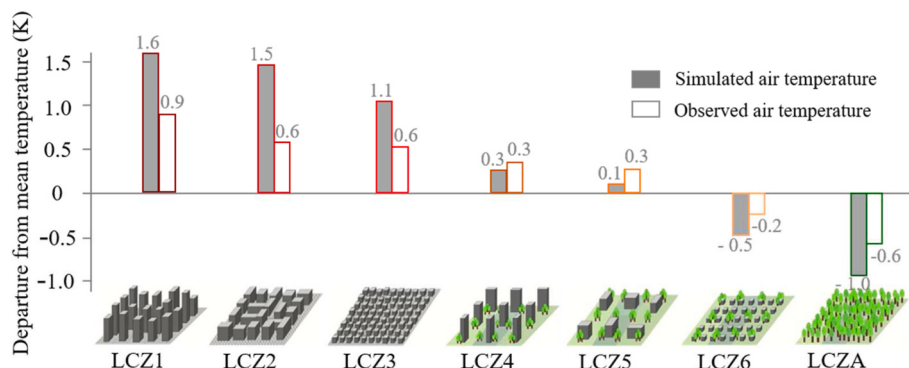


Fig. 13. Thermal difference within local climate zones (LCZs) based on observed air temperatures and simulated air temperatures (generated using the regression model devised in this study).

Funding

This study is supported by Grant from National Natural Science Foundation of China (Grant No. 42071394 and No. 42271477), Guangdong Basic and Applied Basic Research Foundation (Grant No. 2022A1515010171), Guangdong Philosophy and Social Science Foundation (Grant No. GD22CGL38), and the Science and Technology Program of Guangzhou University (Grant No. PT252022006).

CRediT authorship contribution statement

Yong Xu: Writing – review & editing, Writing – original draft, Visualization, Validation, Methodology, Investigation, Funding acquisition, Formal analysis, Data curation, Conceptualization. **Jinxin Yang:** Writing – review & editing, Writing – original draft, Visualization, Validation, Software, Methodology, Investigation. **Yingsheng Zheng:** Writing – review & editing, Writing – original draft, Visualization, Validation, Methodology, Investigation, Funding acquisition, Formal analysis, Conceptualization. **Wenjie Li:** Writing – review & editing, Writing – original draft, Visualization, Software, Methodology.

Declaration of competing interest

The authors declare that they have no known competing financial interests or personal relationships that could have appeared to influence the work reported in this paper.

Data availability

The authors do not have permission to share data.

References

- [1] J.A. Voogt, T.R. Oke, Thermal remote sensing of urban climates, *Rem. Sens. Environ.* 86 (3) (2003) 370–384.
- [2] H.C. Ho, K.K.L. Lau, C. Ren, E. Ng, Characterizing prolonged heat effects on mortality in a sub-tropical high-density city, Hong Kong, *Int. J. Biometeorol.* 61 (2017) 1935–1944.
- [3] W.B. Goggins, E.Y. Chan, E. Ng, C. Ren, L. Chen, Effect modification of the association between short-term meteorological factors and mortality by urban heat islands in Hong Kong, *PLoS One* 7 (6) (2012) e38551.
- [4] E.Y.Y. Chan, W.B. Goggins, J.J. Kim, S.M. Griffiths, A study of intracity variation of temperature-related mortality and socioeconomic status among the Chinese population in Hong Kong, *J. Epidemiol. Community Health* 66 (4) (2012) 322–327.
- [5] Emily YY. Chan, William B. Goggins, Janice SK. Yue, Poyi Lee, Hospital admissions as a function of temperature, other weather phenomena and pollution levels in an urban setting in China, *Bull. World Health Organ.* 91 (8) (2013) 576–584, <https://doi.org/10.2471/BLT.12.113035>. World Health Organization.
- [6] E. Ng, Towards planning and practical understanding of the need for meteorological and climatic information in the design of high-density cities: a case-based study of Hong Kong, *Int. J. Climatol.* 32 (4) (2012) 582–598.
- [7] Z.H. Wang, Reconceptualizing urban heat island: beyond the urban-rural dichotomy, *Sustain. Cities Soc.* 77 (2022) 103581.
- [8] L. Zhao, X. Lee, R.B. Smith, K. Oleson, Strong contributions of local background climate to urban heat islands, *Nature* 511 (7508) (2014) 216–219.
- [9] J.E. Nichol, S.Y. Choi, M.S. Wong, S. Abbas, Temperature change and urbanisation in a multi-nucleated megalopolis: China's Pearl River Delta, *Urban Clim.* 31 (2020) 100592.
- [10] D. Zhou, J. Xiao, S. Bonafoni, C. Berger, K. Deilami, Y. Zhou, J.A. Sobrino, Satellite remote sensing of surface urban heat islands: progress, challenges, and perspectives, *Rem. Sens.* 11 (1) (2018) 48.
- [11] Z. Wu, Y. Xu, Z. Cao, J. Yang, H. Zhu, Impact of urban agglomeration and physical and socioeconomic factors on surface urban heat islands in the Pearl River Delta Region, China, *IEEE J. Sel. Top. Appl. Earth Obs. Rem. Sens.* 14 (2021) 8815–8822.
- [12] D. Fenner, F. Meier, D. Scherer, A. Polze, Spatial and temporal air temperature variability in Berlin, Germany, during the years 2001–2010, *Urban Clim.* 10 (2014) 308–331.
- [13] Q. Chen, R. Liu, Q. Cheng, Y. Chen, S. Cao, M. Du, K. Li, Evaluating the impact of sky view factor and building shadow ratio on air temperature in different residential and commercial building scenarios: a case study of Beijing, China, *Urban Clim.* 49 (2023) 101509.
- [14] W. Zhou, G. Huang, M.L. Cadenasso, Does spatial configuration matter? Understanding the effects of land cover pattern on land surface temperature in urban landscapes, *Landsc. Urban Plann.* 102 (1) (2011) 54–63.
- [15] G. Mills, J. Ching, L. See, B. Bechtel, M. Foley, An introduction to the WUDAPT project, in: *Proceedings of the 9th International Conference on Urban Climate*, 2015, July, pp. 20–24. Toulouse, France.
- [16] E. Ng, C. Yuan, L. Chen, C. Ren, J.C. Fung, Improving the wind environment in high-density cities by understanding urban morphology and surface roughness: a study in Hong Kong, *Landsc. Urban Plann.* 101 (1) (2011) 59–74.
- [17] K.K.L. Lau, C. Ren, Y. Shi, V. Zheng, S. Yim, D. Lai, Determining the optimal size of local climate zones for spatial mapping in high-density cities, in: *Proceedings of the 9th International Conference on Urban Climate Jointly with 12th Symposium on the Urban Environment*, 2015, July, pp. 20–24. Toulouse, France.
- [18] Y. Xu, C. Ren, M. Cai, N.Y.Y. Edward, T. Wu, Classification of local climate zones using ASTER and Landsat data for high-density cities, *IEEE J. Sel. Top. Appl. Earth Obs. Rem. Sens.* 10 (7) (2017) 3397–3405.
- [19] I.D. Stewart, T.R. Oke, Local climate zones for urban temperature studies, *Bull. Am. Meteorol. Soc.* 93 (12) (2012) 1879–1900.
- [20] J. Ching, G. Mills, B. Bechtel, L. See, J. Feddema, X. Wang, N. Theeuwes, WUDAPT: an urban weather, climate, and environmental modeling infrastructure for the anthropocene, *Bull. Am. Meteorol. Soc.* 99 (9) (2018) 1907–1924.
- [21] R. Kotharkar, A. Bagade, Evaluating urban heat island in the critical local climate zones of an Indian city, *Landsc. Urban Plann.* 169 (2018) 92–104.
- [22] Y. Shi, K.K.L. Lau, C. Ren, E. Ng, Evaluating the local climate zone classification in high-density heterogeneous urban environment using mobile measurement, *Urban Clim.* 25 (2018) 167–186.
- [23] J. Emery, B. Pohl, J. Crétat, Y. Richard, J. Pergaud, M. Rega, T. Thévenin, How local climate zones influence urban air temperature: measurements by bicycle in Dijon, France, *Urban Clim.* 40 (2021) 101017.
- [24] S. Jiang, W. Zhan, P. Dong, C. Wang, J. Li, S. Miao, C. Wang, Surface air temperature differences of intra-and inter-local climate zones across diverse timescales and climates, *Build. Environ.* 222 (2022) 109396.
- [25] J. Geletić, M. Lehner, S. Savić, D. Milošević, Inter-/intra-zonal seasonal variability of the surface urban heat island based on local climate zones in three central European cities, *Build. Environ.* 156 (2019) 21–32.
- [26] X. Chen, Y. Xu, J. Yang, Z. Wu, H. Zhu, Remote sensing of urban thermal environments within local climate zones: a case study of two high-density subtropical Chinese cities, *Urban Clim.* 31 (2020) 100568.
- [27] C. Berger, J. Rosentreter, M. Voltersen, C. Baumgart, C. Schmüllius, S. Hese, Spatio-temporal analysis of the relationship between 2D/3D urban site characteristics and land surface temperature, *Rem. Sens. Environ.* 193 (2017) 225–243.
- [28] W.B. Wu, Z.W. Yu, J. Ma, B. Zhao, Quantifying the influence of 2D and 3D urban morphology on the thermal environment across climatic zones, *Landsc. Urban Plann.* 226 (2022) 104499.
- [29] X. Huang, Y. Wang, Investigating the effects of 3D urban morphology on the surface urban heat island effect in urban functional zones by using high-resolution remote sensing data: a case study of Wuhan, Central China, *ISPRS J. Photogrammetry Remote Sens.* 152 (2019) 119–131.
- [30] Y. Chen, J. Wu, K. Yu, D. Wang, Evaluating the impact of the building density and height on the block surface temperature, *Build. Environ.* 168 (2020) 106493.
- [31] Y. Tian, W. Zhou, Y. Qian, Z. Zheng, J. Yan, The effect of urban 2D and 3D morphology on air temperature in residential neighborhoods, *Landsc. Ecol.* 34 (2019) 1161–1178.
- [32] T.M. Logan, B. Zaitchik, S. Guikema, A. Nisbet, Night and day: the influence and relative importance of urban characteristics on remotely sensed land surface temperature, *Rem. Sens. Environ.* 247 (2020) 111861.
- [33] L. Chen, E. Ng, X. An, C. Ren, M. Lee, U. Wang, Z. He, Sky view factor analysis of street canyons and its implications for daytime intra-urban air temperature differentials in high-rise, high-density urban areas of Hong Kong: a GIS-based simulation approach, *Int. J. Climatol.* 32 (1) (2012) 121–136.
- [34] Y. Zheng, C. Ren, Y. Shi, S.H. Yim, D.Y. Lai, Y. Xu, W. Li, Mapping the spatial distribution of nocturnal urban heat island based on Local Climate Zone framework, *Build. Environ.* 234 (2023) 110197.
- [35] F. Guo, Q. Wu, U. Schlink, 3D building configuration as the driver of diurnal and nocturnal land surface temperatures: application in Beijing's old city, *Build. Environ.* 206 (2021) 108354.
- [36] F. Guo, U. Schlink, W. Wu, D. Hu, J. Sun, Scale-dependent and season-dependent impacts of 2D/3D building morphology on land surface temperature, *Sustain. Cities Soc.* 97 (2023) 104788.
- [37] Y. Xu, C. Ren, P. Ma, J. Ho, W. Wang, K.K.L. Lau, E. Ng, Urban morphology detection and computation for urban climate research, *Landsc. Urban Plann.* 167 (2017) 212–224.
- [38] S. Tong, N.H. Wong, S.K. Jusuf, C.L. Tan, H.F. Wong, M. Ignatius, E. Tan, Study on correlation between air temperature and urban morphology parameters in built environment in northern China, *Build. Environ.* 127 (2018) 239–249.
- [39] Y. Zheng, C. Ren, Y. Xu, R. Wang, J. Ho, K. Lau, E. Ng, GIS-based mapping of Local Climate Zone in the high-density city of Hong Kong, *Urban Clim.* 24 (2018) 419–448.
- [40] J.C. Jiménez-Muñoz, J.A. Sobrino, D. Skoković, C. Mattar, J. Cristobal, Land surface temperature retrieval methods from Landsat-8 thermal infrared sensor data, *Geosci. Rem. Sens. Lett. IEEE* 11 (10) (2014) 1840–1843.
- [41] A. Gillespie, S. Rokugawa, T. Matsunaga, J.S. Cothorn, S. Hook, A.B. Kahle, A temperature and emissivity separation algorithm for advanced Spaceborne thermal emission and reflection radiometer (ASTER) images, *IEEE Trans. Geosci. Rem. Sens.* 36 (4) (1998) 1113–1126.
- [42] G.C. Hulley, F.M. Götsche, G. Rivera, S.J. Hook, R.J. Freepartner, M.A. Martin, W.R. Johnson, Validation and quality assessment of the ECOSTRESS level-2 land surface temperature and emissivity product, *IEEE Trans. Geosci. Rem. Sens.* 60 (2021) 1–23.

- [43] C. Yan, Q. Guo, H. Li, L. Li, G.Y. Qiu, Quantifying the cooling effect of urban vegetation by mobile traverse method: a local-scale urban heat island study in a subtropical megacity, *Build. Environ.* 169 (2020) 106541.
- [44] J. Yang, Q. Shi, M. Menenti, Y. Xie, Z. Wu, Y. Xu, S. Abbas, Characterizing the thermal effects of vegetation on urban surface temperature, *Urban Clim.* 44 (2022) 101204.
- [45] Y. Chen, J. Yang, R. Yang, X. Xiao, J.C. Xia, Contribution of urban functional zones to the spatial distribution of urban thermal environment, *Build. Environ.* 216 (2022) 109000.